Elastic scattering of $^{16}O+^{16}O$ at energies E/A between 5 and 8 MeV

M. P. Nicoli, F. Haas, R. M. Freeman, N. Aissaoui, C. Beck, A. Elanique, and R. Nouicer
Institut de Recherches Subatomiques, UMR7500, CNRS-IN2P3 and Université Louis Pasteur, Boîte Postale 28, F-67037 Strasbourg Cedex 2, France

A. Morsad
Faculté des Sciences Ben M'Sik, Université Hassan II, Casablanca, Morroco

S. Szilner and Z. Basrak
Ruđer Bošković Institute, Zagreb, Croatia

M. E. Brandan
Instituto de Física, Universidad Nacional Autónoma de México, Apartado Postal 20-364, México 01000 DF, Mexico

G. R. Satchler
Department of Physics and Astronomy, University of Tennessee, Knoxville, Tennessee 37996 and Physics Division, Oak Ridge National Laboratory, Oak Ridge, Tennessee 37831-6373
(Received 29 April 1999; published 15 November 1999)

The elastic scattering of $^{16}O+^{16}O$ has been measured at nine energies between $E_{lab}=75$ and 124 MeV. The data cover up to 100° in the c.m. and can be described in terms of phenomenological and folding model potentials which reproduce the main features observed. In agreement with studies at higher energies in this and similar systems, refractive effects are present in the angular distributions at all energies. In particular, the passage of Airy minima through 90° at $E_{c.m.}=40$, 47.5, and 62 MeV explains the deep minima observed in the excitation function. The real part of the optical potential is found to vary very little with energy over the studied interval, but the imaginary part shows a rapid change in its shape at incident energy about 90 MeV. Nonetheless, the energy dependence of the volume integral of the real and imaginary parts is in agreement with dispersion relation predictions. [S0556-2813(99)05611-3]

PACS number(s): 25.70.Bc, 24.10.Ht

I. INTRODUCTION

In recent years, our understanding of the main features of the nuclear optical potential for light heavy ions has advanced enormously. Very complete measurements of the elastic scattering at various energies and in different systems have shown the presence of strong refractive effects in the angular distributions. The optical model analysis of these data in terms of phenomenological and microscopic potentials has consistently resulted in potentials featuring a deep real part associated with a rather weak absorption. Recent reviews of the theoretical and experimental state-of-the-art in this field can be found in Refs. [1,2].

Nuclear rainbows and their accompanying Airy interference patterns, first identified in a ''heavy-ion'' interaction by Goldberg and Smith in ^{4}He elastic scattering on heavier nuclei [3], have later been observed in the interaction induced by ^{6}Li, ^{7}Li, ^{12}C, and ^{16}O ions. Among these, the most remarkable nuclear rainbows have been the ones observed in the system $^{16}O+^{16}O$ at energies E/A near and above 8 MeV [4–9]. The presence of the refractive Airy structure in all these measurements has permitted a rather unambiguous description of the data using phenomenological potentials whose parameters vary continuously as a function of the incident energy, and whose real and imaginary volume integrals are related by the energy dependence expected from dispersion relation predictions [10,11]. Also, ''hybrid'' analyses using microscopic real potentials together with phenomenological imaginary parts, have been successful [6,7], describing the data with renormalizations of the calculated potential close to unity, and imaginary parts fully consistent with the purely phenomenological studies.

The lowest energy where refractive effects have been identified and studied in the $^{16}O+^{16}O$ elastic-scattering angular distribution is 124 MeV [9]. This energy coincides with one of the very deep minima in the 90° excitation function [12], and the optical model analysis has permitted one to explain this feature [9] as arising from the presence of an Airy minimum at that angle. A similar analysis for $^{12}C+^{12}C$ has described [13] in the same terms the gross structure in its excitation function above $E_{c.m.}=35$ MeV [14,15]. At lower energies, below $E/A=5$ MeV, the extremely weak absorption (which can be understood by the small number of open channels in these reactions [16]) has allowed the observation of resonances in the excitation function [17] of this and other systems involving the closed- or semi-closed- shell nuclei ^{12}C, ^{14}C, ^{15}N, and ^{16}O.

In this work we report elastic-scattering angular distributions measured for $^{16}O+^{16}O$ between 10° and 100° at nine different energies between 75 and 124 MeV. The chosen energies include those showing either maxima or minima in the 90° excitation function [12]. The small-angle measurements were performed using a Q3D magnetic spectrometer with a position-sensitive (PS) proportional counter in its fo-

cal plane, and two PS silicon detectors in kinematical coincidence at the larger angles. The good statistics required to perform a detailed data analysis have been attained at all angles and energies.

The results of the present optical model analysis, which is done assuming either phenomenological or microscopic real potentials, allow a better understanding of the energy evolution of the potential at these medium energies, show the persistence of the refractive phenomena down to $E/A = 4.7$ MeV, and offer a mean-field explanation for the gross structure in the excitation function. A preliminary report on this work can be found in Ref. [18].

II. EXPERIMENTAL DETAILS

The $^{16}O+^{16}O$ elastic scattering has been measured at $E_{lab}=75.0$, 80.6, 87.2, 92.4, 94.8, 98.6, 103.1, 115.9, and 124.0 MeV with a beam provided by the Strasbourg Tandem Vivitron accelerator. This facility is perfectly suited for studies in the intermediate energy domain, E/A between 5 and 10 MeV, which may require frequent and precise changes of bombarding energies. The oxygen targets, ~ 20 μg/cm^2 thick self-supporting BeO films, were produced at the accelerator laboratory following techniques developed locally [19]. The choice of a light oxide such as BeO as the target has a number of advantages since it allows a relatively good spectral separation between the ^{16}O nuclei scattered off ^{9}Be and ^{16}O and also, the forward focusing of the yields from ^{9}Be suppresses their contribution at the larger angles. It is worth mentioning that ^{9}Be has no excited bound states, which greatly simplifies the interpretation of the ^{16}O inelastic-scattering spectrum. The oxygen content of the targets was determined in two independent measurements: by Rutherford backscattering of 2 MeV ^{4}He ions, and by a comparison between the large angle yields in the (equal $E_{c.m.}$ reactions) $^{12}C(E_{lab}=60$ MeV$)+^{16}O$ and $^{16}O(E_{lab}=80$ MeV$)+^{12}C$ elastic scattering off a ^{12}C target of known thickness.

Detailed and complete angular distributions have been measured at all energies. The most forward angles ($5° \leqslant \theta_{lab} \leqslant 20°$) of a given angular distribution were covered by a Q3D magnetic spectrometer having a proportional counter at its focal plane. Spectrometer measurements were taken every $\Delta\theta_{lab}=0.5°$. The cross sections at larger angles were measured by a fixed kinematical-coincidence setup consisting of two position-sensitive silicon detectors (area $=5 \times 1$ cm^2) placed 7.8 cm from the target, on both sides of the beam, and covering angles between 15° and 50°, and $-35°$ and $-70°$, respectively. The electronics and data acquisition systems for the proportional counter and the silicon detectors were independent from each other. The dead time of both systems was monitored and kept as constant as possible by changing the spectrometer entrance slits and/or the beam intensity. About 50 different measurements could be performed at forward angles with the Q3D spectrometer while accumulating the data in the silicon detectors.

All details concerning the data reduction, in particular the identification of the elastic channel in both detection systems and the extraction of cross sections can be found in Ref. [20]. Final normalization of the absolute cross sections was determined by comparing the measurements at the most forward angles, $\theta_{lab}<10°$ where Mott scattering dominates, with optical model predictions which in this angular region are only weakly dependent on potential parameters. Excellent agreement is found between our 124 MeV data and those by Kondo [9] at the same energy. Angular distributions between $\theta_{c.m.}=10°$ and 100° could be measured with good statistics at all energies of this study. The distribution is symmetric about $\theta_{c.m.}=90°$ for this identical-boson system.

III. OPTICAL MODEL ANALYSIS

A. Phenomenological potentials

In this work we have assumed, in accordance with previous phenomenological analyses of the $^{16}O+^{16}O$ system [5,6,9], the squared Woods-Saxon shape, WS2, for the potential real part and the sum of a WS2 ''volume'' term, plus a derivative Woods-Saxon (WSD) ''surface'' term, for the imaginary potential. The phenomenological nuclear potential $U_{ph}(r)$ is, then,

$$U_{ph}(r) = -V[f_V(r)]^2 - iW[f_W(r)]^2 - iW_D f_D(r), \quad (1)$$

where the Woods Saxon terms are

$$f_{V,W}(r) = \left[1+\exp\left(\frac{r-R_{V,W}}{a_{V,W}}\right)\right]^{-1}, \quad (2)$$

and the derivative term is

$$f_D(r) = -4a_D\frac{d}{dr}\left[1+\exp\left(\frac{r-R_D}{a_D}\right)\right]^{-1}. \quad (3)$$

In general, for an interaction potential U_E(r) between nuclei having nucleon numbers A_1 and A_2, the volume integral per interacting nucleon pair, J_U, is defined as

$$J_U(E) = -\frac{4\pi}{A_1A_2}\int U_E(r)r^2dr. \quad (4)$$

This quantity is currently used as a sensitive measure of the potential strength. In this work we apply this definition to the real and to the imaginary parts of $U(r)$ independently, and call the resulting volume integrals ''J_V'' and ''J_W,'' respectively.

The optical model analysis at each energy was done using the code PTOLEMY [21], with a Coulomb potential calculated as the interaction between two uniformly charged spheres of radii equal to 3.54 fm. The automatic search optimized the fit to the data by minimizing the χ^2 function, defined as

$$\chi^2 = \frac{1}{N}\Sigma_{i=1}^{N}\frac{(\sigma_t-\sigma_e)^2}{(\Delta\sigma_e)^2}, \quad (5)$$

where σ_t, σ_e, and $\Delta\sigma_e$ are the theoretical cross sections, the experimental cross sections, and the uncertainties in the experimental cross sections, respectively. N is the number of angles at which measurements have been carried out. The uncertainties were set to be a fixed percentage (10%) of the

experimental cross section, for all measurements. In this way, the angles close to 90°, where the experimental uncertainty can be relatively large due to the smaller cross section, have a sufficient weight to influence the fit. At some energies, particularly where the search ended with a fit that we would not consider as sufficiently good, we attempted improving the overall agreement by modifying the criterion for the uncertainties. We concluded that assuming a uniform percentage was appropriate.

Preliminary attempts to fit the higher energy data sets showed the appearance of discrete ambiguities in the real potential determination. For instance, at 116 MeV, equally good fits could be obtained with real potentials having central depths V equal to 367, 412, or 456 MeV, and corresponding J_V equal to 297, 333, and 375 MeV fm^3, respectively. This inconvenience, which has appeared in the analyses of other systems at similar energies, has been thoroughly addressed by Kondo *et al.* at 124 and 145 MeV [5,9], who have argued in favor of one particular family (''family IV,'' having a volume integral equal to 337 MeV fm^3 at 124 MeV) as being the ''correct'' one. Kondo's preference, which is based on continuity arguments, takes into account results from various analyses of $^{16}O+^{16}O$ data, in particular, the remarkable nuclear rainbow observed at 350 MeV [4]. Because of the value of their volume integrals, the three potentials encountered in our analysis belong to families III, IV, and V, respectively, in Kondo's nomenclature [9].

Each of these families of real potentials has, at 124 MeV, an associated real radius R_V approximately equal to 3.92, 3.97, and 4.03 fm, respectively [9]. It was found that fixing the real radius to these values helped enormously to stabilize the automatic search within a given family, without affecting the quality of the fit. Thus, the analysis was performed by keeping the real radius fixed at the given values for each of the three investigated families, and optimizing the fit to the data through an automatic search on the remaining two real and the six imaginary potential parameters.

B. Microscopic potentials

Energy- and density-dependent effective nucleon-nucleon interactions have been used to generate microscopic real potentials which, associated with phenomenological imaginary terms, successfully describe light heavy-ion elastic-scattering data at intermediate energies [2]. The degree of success of the model is indicated by the potential renormalization required to give an optimum fit to the measurements. This renormalization should be close to unity. The ''BDM3Y1(Paris)'' effective interaction, proposed by Khoa and von Oertzen [22], has been shown to describe a wide set of light heavy-ion elastic-scattering data [6,7], in particular the $^{16}O+^{16}O$ measurements at 145, 250, 350, and 480 MeV, with energy-independent renormalizations of the order of 0.90 ± 0.03 [6]. Thus, our folding model analysis has assumed a nuclear potential $U_{\rm fm}(r)$, such that

$$U_{\rm fm}(r)=N_{\rm V}f_{\rm BDM3Y1}(r)-iW[f_W(r)]^2-iW_Df_D(r), \quad (6)$$

where the $f_{\rm BDM3Y1}(r)$ term is a microscopic real potential obtained by double convolution between the BDM3Y1(Paris) effective interaction and the two ^{16}O density distributions. The ^{16}O density distribution was represented by a two-parameter Fermi function with a radius of 2.60 fm and a diffuseness of 0.45 fm. These parameters give a root-mean-squared (rms) charge radius which agrees with electron-scattering results [23]. The parameter N_V is the overall renormalization of the real potential which is adjusted to optimize the fit and which is expected to be close to unity. The volume and surface imaginary terms are defined in the same way as was done in the phenomenological study. Thus a total of seven parameters (one for the real part and the six parameters defining the imaginary terms) were left free in this analysis. The automatic optimization of the parameters was done using the code PTOLEMY following the same criteria for the Coulomb interaction and the treatment of uncertainties as described in the previous subsection.

The BDM3Y1 interaction shows a weak energy dependence over the energy interval covered in this study. At 75 MeV, the calculated potential (without renormalization) has a J_V of 387.6 MeV fm^3 and a rms radius of 4.214 fm. At 124 MeV these values are 379.0 MeV fm^3 and 4.216 fm, respectively. That is, a 2% variation in integrated strength for a 65% increase in energy. For simplicity, we have performed our analysis using, at all energies, the $f_{\rm BDM3Y1}$ potential calculated for 124 MeV.

IV. RESULTS OF THE ANALYSIS

A. Phenomenological potential results

Figure 1 shows the data and the optical model fits obtained with phenomenological potentials (dash curves) whose parameters are listed in Table I. To be consistent with Kondo's extensive analyses of this system [5,9,24] we have chosen to show the ''family IV'' of real potentials ($J_V = 337$ MeV fm^3 at 124 MeV). The fits obtained with potentials belonging to families III and V are generally indistinguishable from those being presented here. As Fig. 1 shows, the calculations describe well the main features of the measurements, even though one observes a systematic deficiency at the forward angles. The structures at the intermediate angles are generally well reproduced, and the theoretical interference near 90° follows closely the measurements. Table I indicates that the WS2 real part does not display any systematic dependence with energy, having a volume integral J_V on the average equal to 344 ± 11 MeV fm^3.

Previous analyses [6,9] of Sugiyama's *et al.* measurements at 124 MeV have shown that an acceptable description of the data was possible with just the volume term for the imaginary part. The same can be said for these data at the highest three energies. However, at 99 MeV and below, the fits demanded greater flexibility in the potential. It was found that allowing for a surface imaginary term WSD in addition to the WS2 resulted in a good agreement with the lower energy data and, for consistency, the data at all the energies were analyzed in the same way. In general, the parameters of the fit were well determined by the data at the higher and lower energies of this study. However, at bombarding energies about 95 MeV, where the transition between two differ-

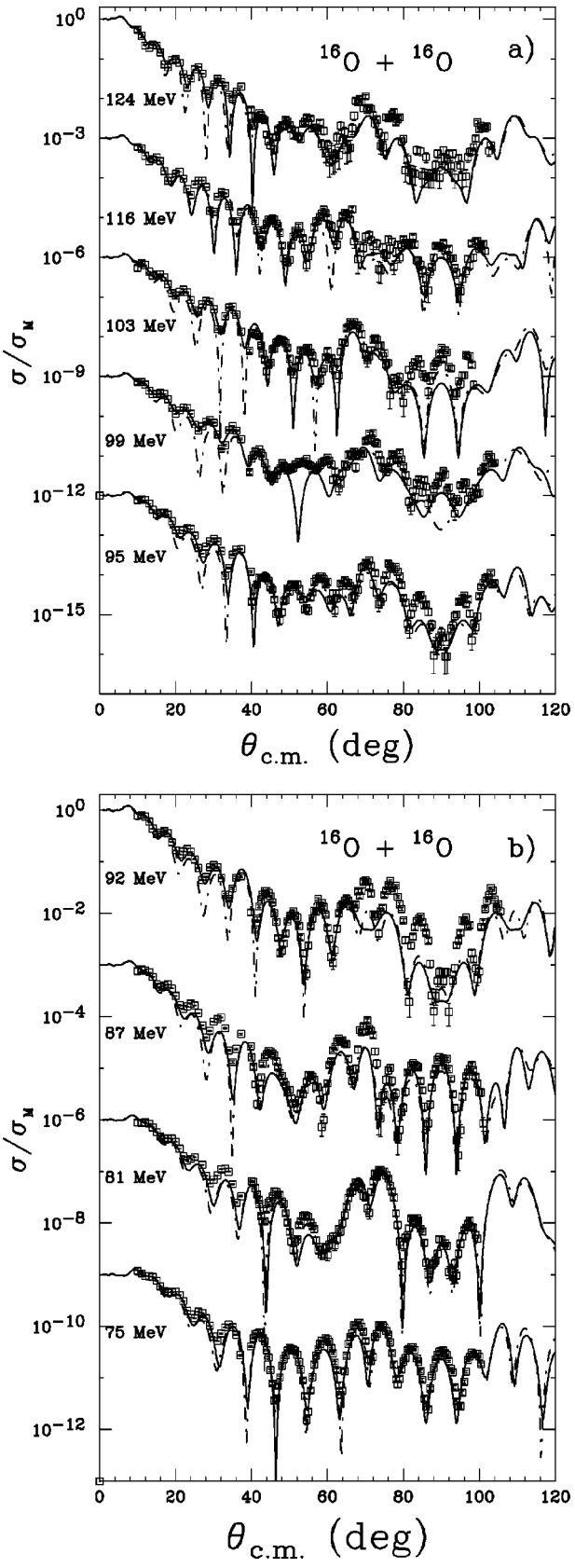

FIG. 1. Elastic-scattering data and optical model calculations with phenomenological (dash, Table I) and microscopic (solid, Table II) potentials. Data at different energies have been displaced by factors of 10^{-3}, for clarity.

ent types of potentials is taking place, it was possible to reach equally acceptable descriptions with more than one set of parameters. These alternative solutions all shared the general features we are reporting, and whenever a choice was necessary, the regularity of the parameters from one energy to the next was the applied criterion.

The best fits at the three lowest energies consistently seemed to require very small values of the imaginary volume diffuseness a_W, in some cases, smaller than 0.10 fm. To avoid possible reflections from such extremely thin-skinned potentials we report potentials where the value of a_W was maintained fixed at 0.20 fm during the search. The values of χ^2 for the optimum fits are about 17, 9, and 9, at 87.2, 80.6, and 75 MeV, respectively. The main differences between the optimum fits and those shown in Fig. 1(b) are the depth of the Fraunhofer minima at forward angles, the calculations with smaller values of a_W being in better agreement with the relatively shallow experimental minima, and the description of the interference structures at intermediate angles. In Table I the values of a_D at the two highest energies were also kept fixed during the search to prevent extremely low values which minimized χ^2. Since the derivative term is a weak component of the absorption at these energies, restricting a_D to 0.20 fm does not affect the quality of the fits. The chosen limiting values for the diffuseness are comparable to the system's asymptotic reduced wavelength $\lambda\!\!\!^{-}$ (typically, 0.24 fm); however, we note that the local $\lambda\!\!\!^{-}$ inside the deep real potential is significantly smaller than this.

Figure 2 shows the imaginary potential for three different energies, as typical representatives of the results found at the high, medium, and low range of this study. The imaginary potential at 124 MeV is mostly of the volume type, the weak surface term is located at 7.4 fm and represents less than 0.1% of the total imaginary volume integral. At 75 MeV, quite a different situation has set in. The derivative term now contributes 22% of the total volume integral J_W, and it is located near 7 fm [which can be considered as the surface of the system, about 1.4 times $(16^{1/3}+16^{1/3})$ fm]. At the same time, the volume term has taken on a relatively thin edge and is limited to be within the central region [R_W is about 1.0 times $(16^{1/3}+16^{1/3})$] fm. The potential shown in Fig. 2 for 95 MeV, a medium energy in this study, is intermediate between the two extreme situations. In Fig. 2 we also show the tail of the real potential needed to fit the 124 MeV data (which, in fact, is quite similar to that needed at all energies). As can also be observed, the imaginary potential is weaker than the real one at all radii.

Alternative descriptions of the lower energy measurements were attempted, in particular the use of a simple three-parameter volume imaginary potential. In this case, the evolution in the shape of the volume term for energies lower than 99 MeV manifested itself in a sudden change of $W(r)$ towards an almost exponentially decaying absorption, about 25 MeV deep at the center and a half-value-thickness of about 2–3 fm (typical WS2 parameters: 51 MeV, 2.7, and 2.6 fm). This potential produced fits of poorer quality than the ones shown in Fig. 1. Remarkably, the volume integrals J_W of these ''exponential'' imaginary potentials were similar to the integrals of their corresponding WS2 plus WSD coun-

TABLE I. Phenomenological potentials. The real part is a WS2 term with real radius $R_V=3.97$ fm, and the imaginary part is the sum of a WS2 plus a WSD term. Underlined parameters were kept fixed during the search.

Energy [a] (MeV)	V (MeV)	a_V (fm)	J_V (MeV fm^3)	W (MeV)	R_W (fm)	a_W (fm)	W_D (MeV)	R_D (fm)	a_D (fm)	J_W (MeV fm^3)	σ_R [b] (mb)	χ^2
124.0	418	1.568	344	15.3	7.07	0.920	0.028	7.40	0.20	66.9	1713	28
115.9	419	1.440	333	12.2	7.13	0.624	0.392	7.22	0.20	59.2	1513	25
103.1	420	1.563	345	11.2	7.08	0.446	0.944	7.42	0.280	57.8	1520	28
98.6	412	1.431	326	14.2	6.66	0.860	0.262	7.96	0.220	58.7	1545	23
94.8	418	1.555	342	12.6	6.60	0.601	1.75	6.74	0.460	54.7	1506	27
92.4	423	1.556	347	9.34	7.24	0.333	1.25	7.49	0.119	52.7	1450	28
87.2	420	1.450	334	16.6	4.77	0.20	3.46	6.41	0.527	41.2	1527	30
80.6	414	1.510	335	14.4	5.00	0.20	1.98	7.00	0.517	36.6	1550	13
75.0	423	1.517	343	11.4	5.17	0.20	1.96	7.00	0.334	29.4	1382	9.1

[a]The laboratory energy.
[b]The total reaction cross section.

terparts. We also tried fitting the data with potentials of WS shape raised to powers other than 2, but no systematic improvement was noticed. The surface-peaked derivative term in the absorption is apparently required for the best fits to the data.

The value of the absorption at large radii, mostly determined by the imaginary diffuseness and radius, may strongly affect the calculated total reaction cross sections σ_R given in Table I. At energies where a_W and a_D have been restricted, we have confirmed that the listed values of σ_R are not too dependent on the imposed limits. The agreement between values is always better than about 25 mb. This ''uncertainty'' is comparable to the variations found among alternative potential parameters.

B. Microscopic potential results

Similar to what was reported in a previous study of the identical nuclei system $^{12}C+^{12}C$, with elastic scattering between 75 and 126 MeV [25], discrete ambiguities were also found here in the determination of the optimum renormalization N_V of the real folded potential. For instance, at 116 MeV, good fits (in terms of their χ^2) and rather indistinguishable from each other (when judged visually) could be obtained with the folded potential $f_{\mathrm{BDM3Y1}}(r)$ renormalized by 0.78, 0.90, and 1.06 (corresponding to J_V equal to 303, 342, and 401 MeV fm^3, respectively). Following the results of Khoa *et al.* [6], who fitted $^{16}O+^{16}O$ data obtained at higher energies with BDM3Y1 folding model potentials renormalized by about 0.9, we have chosen the $N_V\approx 0.9$ family of solutions. Furthermore, their volume integrals coincide quite exactly with the independently chosen phenomenological family IV of Kondo.

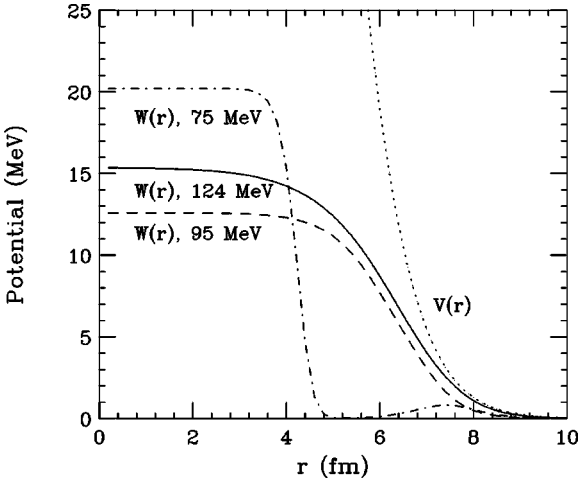

FIG. 2. The imaginary potential (parameters in Table I) at the three indicated bombarding energies. The dotted curve shows the real potential at $E_{\mathrm{lab}}=124$ MeV.

Solid curves in Fig. 1 show the fits obtained in the folding model analysis of the data and Table II lists the parameters that determine the potential. The same restrictions explained above were imposed on the values of the volume imaginary diffuseness at the lower energies, and its qualitative effect on the data description is similar to that found in the phenomenological analysis. Imposing the restriction $a_W=0.20$ fm at 87.2 MeV causes the derivative term to adopt a diffuseness larger than the one in the best fit (of the order of 0.5–0.6 fm), in turn increasing the value of the calculated σ_R by about 300 mb with respect to the optimum value, close to 1470 mb. In this only case, we consider the listed value as highly uncertain.

As can be observed in Fig. 1, the fits with microscopic potentials are quite similar to those obtained in the phenomenological analysis, except that the Fraunhofer oscillations at forward angles are better described by the microscopic potential, while the latter potential is less successful than the former in the intermediate angles description. The real part volume integrals do not display any systematic energy dependence, and the average renormalization is $N_V=0.90\pm0.02$ (average $J_V=343$ MeV fm^3).

Figure 3 shows the phenomenological and the microscopic real potentials that fit the 124 MeV data. They agree quite closely with each other up to $r=6$ fm, but with the microscopic potential being less diffuse than the WS2 one at

TABLE II. Microscopic potentials. The real part is the folded potential times N_V, and the imaginary is the sum of a WS2 and a WSD term. Underlined parameters were kept fixed during the search.

Energy (MeV)	N_V	J_V (MeV fm^3)	W (MeV)	R_W (fm)	a_W (fm)	W_D (MeV)	R_D (fm)	a_D (fm)	J_W (MeV fm^3)	σ_R (mb)	χ^2
124.0	0.89	337	15.4	7.05	0.940	0.023	7.50	0.20	66.2	1681	31
115.9	0.90	342	14.5	6.92	0.846	0.141	8.69	0.143	60.1	1589	17
103.1	0.91	344	11.8	7.09	0.489	1.078	7.48	0.270	60.8	1516	32
98.6	0.93	351	11.0	7.42	0.490	0.553	8.15	0.295	63.7	1609	26
94.8	0.88	332	14.0	6.20	0.650	1.743	6.89	0.551	51.4	1559	23
92.4	0.91	343	8.92	7.26	0.430	0.978	7.64	0.127	49.1	1444	30
87.2	0.89	336	17.2	4.90	0.20	1.965	6.72	0.803	44.2	1765[a]	33
80.6	0.89	336	18.1	4.31	0.20	1.392	7.23	0.598	29.6	1592	15
75.0	0.90	340	20.2	4.39	0.20	0.827	7.41	0.446	28.6	1403	12

[a]Uncertain value, see the text.

larger radii. Probably it is this difference that causes the improved folding model fits at the forward angles observed in Fig. 1. The overall agreement between the two types of potentials explains the coincidence of their volume integrals, as well as the similar general features of the imaginary potentials that accompany either description. Our observations on the strong evolution with the energy of the imaginary part associated with the WS2 real potential, also apply here when the folded potential is used.

V. INTERPRETATION OF THE RESULTS IN TERMS OF AIRY MINIMA

The angular distributions shown in Fig. 1 are extremely complicated to interpret, not only because the weak absorption permits a strong interference among many partial waves, but also because the indistinguishibility of the two participating nuclei produces an additional quantum interference about 90°. The near-far decomposition technique, first presented by Fuller [26], has proven to be of great help unraveling the interference caused by trajectories originating from different sides of the scattering potential. The convention states that trajectories being scattered into the same side from whence they came belong to the ''nearside,'' whereas trajectories scattered to the opposite side of the target are the ''farside'' ones [27,28]. As an example of its power, the method has recently furnished a simple mean-field explanation of the deep minima observed in the 90° excitation function of the $^{12}C+^{12}C$ system [13].

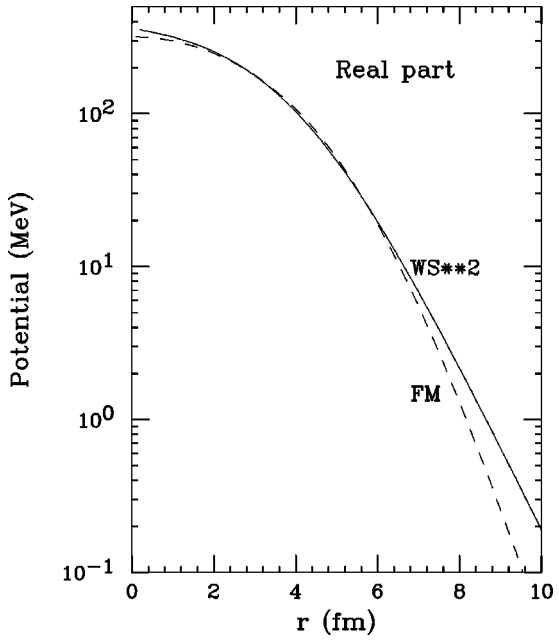

FIG. 3. The real potential. Comparison between the folding model (dash curve) and the WS2 (full curve) real parts at $E_{\rm lab}=124$ MeV.

In order to simplify the analysis of these results, all the near-far calculations we present have artificially eliminated the identical-particle symmetrization of the angular distribution. Figure 4 shows the near-far decomposition of two angular distributions calculated with the microscopic potentials listed in Table II. The difference between the (total) cross section in Fig. 4 and those shown in Fig. 1 is due to the near-far calculation not being symmetrized. The curves for 124 MeV in Fig. 4 display the main features that have already been encountered in previous studies of this and other similar systems at higher energies: the angular distribution is dominated at small angles, in this case up to $\approx 50°$, by the Fraunhofer interference between near and farside amplitudes, and at larger angles by the structure in the rainbow scattering due to the refractive Airy interference between two subamplitudes of the farside scattering. At the most backward angles, hints of the ''glory'' effect, caused by the farside trajectory going around past 180° [28], are noticeable.

The calculation at 75 MeV in Fig. 4 shows a rather different pattern since the Fraunhofer oscillations seem to extend all the way to 180°. At forward angles, the interference is quite similar to that observed at the higher energies, but beyond $\approx 80°$, the decaying nearside amplitude recovers its strength due to a totally different effect. The farside, due to the weak absorption and, possibly, to the particular shape of the imaginary potential at these energies, decreases slowly with angle, and after passing through 180° goes around (therefore, deserving to be considered ''nearside'' by the

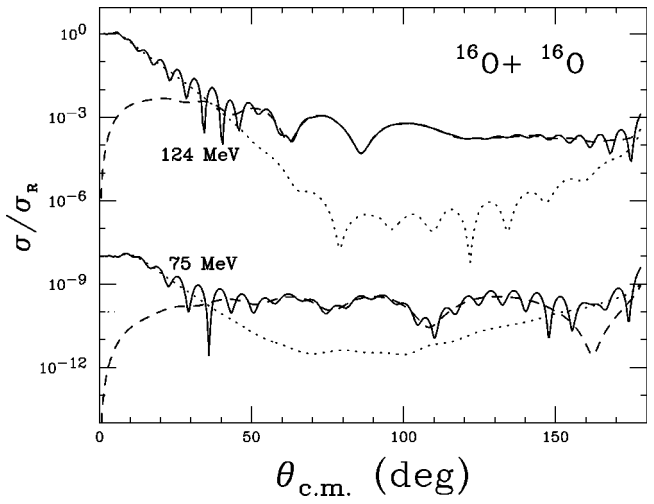

FIG. 4. Near-far decomposition of two typical angular distributions encountered in this study, one at high energies ($E_{lab}=124$ MeV) and one at low energies ($E_{lab}=75$ MeV). The calculations are unsymmetrized and done with the folding model potentials. The solid curve shows the total calculation, while the dotted and dashed curves show the nearside and the farside, respectively. The calculations at 75 MeV have been displaced by a factor of 10^{-8}, for clarity.

convention) and interferes with the farside forward of 180° in an extended backward glory which dominates the angular distribution between 80° and 180°. So, if technically all these oscillations are nearside-farside interferences, only at forward angles are they of diffractive origin, the rest being caused by nuclear refraction.

Figure 5 shows results from the near-far decomposition at all the energies in this study. We have performed the decomposition assuming the microscopic real potential (Table II) together with an imaginary part equal to one-half of the volume term required by the data. In this way, we emphasize the effect of the real potential on the angular distribution, and thus facilitate the task of identifying the structures of refractive origin. To further simplify the presentation we show in Fig. 5 only the farsides. A rather smooth energy evolution can be appreciated in all of the displayed angular distributions. Since the real potential is very weakly dependent on the energy, the evolution of the refractive Airy pattern is almost all due to the change in wavelength. Following Kondo [5,9] who has systematically studied the evolution of $^{16}O+^{16}O$ Airy minima with bombarding energy, we identify the 90° Airy minimum near 124 MeV as A_3, where the subscript denotes the order of the minimum, that is, the third minimum forward of the nuclear rainbow. According to our results in Fig. 5, A_4, located at about 62° at 124 MeV, moves backwards as the energy diminishes and passes through 90° near 99 MeV (the data themselves show a 90° minimum near 95 MeV, but our fits do not exactly reproduce the feature). The minimum A_5 evolves similarly until it crosses 90° at about 80 MeV.

As Rowley *et al.* emphasized in 1977 [29], a 90° cross section minimum in an identical-boson system such as this one, can only be caused by a minimum in the unsymmetrized amplitude. This, in turn, can arise from a deep Airy minima

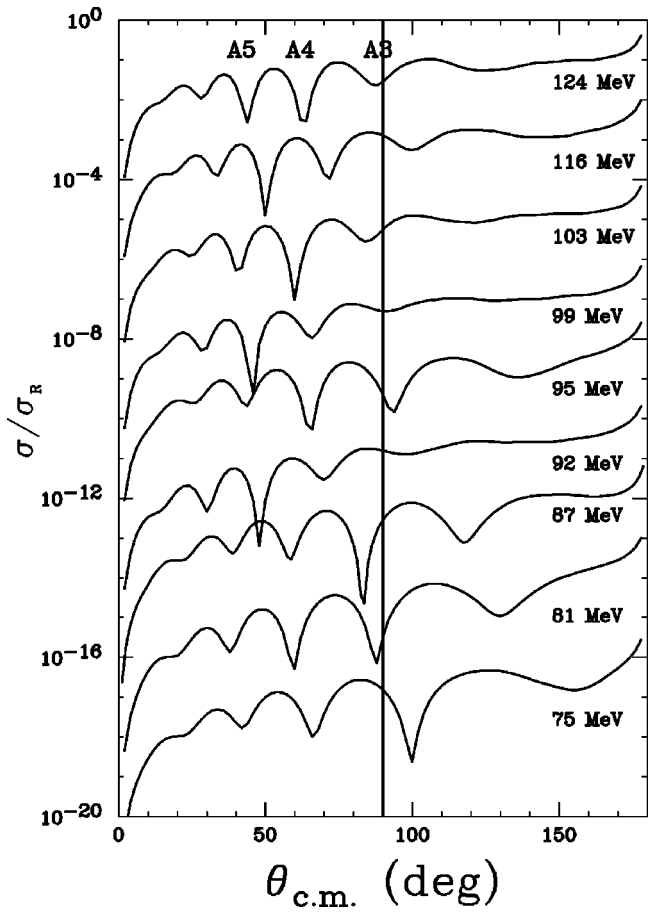

FIG. 5. Farsides calculated for all measured energies. The imaginary part has been reduced to emphasize the refractive effects. The calculations are unsymmetrized. Curves at different energies have been displaced by factors of 10^{-2}, for clarity.

present at 90° in a farside-dominated angular distribution. Therefore, we expect that the Airy minima identified in Fig. 5 might be visible in the 90° excitation function. Excitation function data have been obtained for $^{16}O+^{16}O$ at energies similar to the ones in this study at ORNL [12], and deep minima appear at $E_{c.m.}$ equal to 40, 47.5, 54, and 62 MeV, corresponding to 80, 95, 108, and 124 MeV in the laboratory. From our analysis, we propose that three of these excitation function minima have a refractive origin and that they correspond to A_3 at $E_{c.m.}=62$ MeV, A_4 at $E_{c.m.}=47.5$ MeV, and A_5 at $E_{c.m.}=40$ MeV. We remind the reader that A_2 is believed to be the minimum observed in the excitation function at $E_{c.m.}=75$ MeV, and A_1 is predicted to cross 90° at about 100 MeV [9]. The minimum observed in the excitation function at $E_{c.m.}=54$ MeV [12] can be due to the interference caused by the angular distribution symmetrization: it is observed in the cross section as a function of the energy, but not in the angular distribution.

VI. DISCUSSION OF RESULTS

The results being presented show that this complete set of new data at incident energies between 75 and 124 MeV can be described by real potentials which are similar to those

needed at higher energies in this and other light heavy-ion systems. The analyses with phenomenological and microscopic potentials end up with similar and mutually consistent results, with the latter giving a better description of the data at forward angles. These potentials are deep, 300–400 MeV at the center. They have volume integrals of ≈ 340 MeV fm^3 and rms radii ≈ 4.2–4.4 fm. The renormalization required for the BDM3Y1 microscopic potential, is on the average 0.90, similar to results found at higher energies. A recent folding model analysis [30] was undertaken of the available data for this system at bombarding energies ranging from 124 to 1120 MeV. This data set included the 124 and 145 MeV data measured by Sugiyama *et al.* [5,9]. The authors of Ref. [30] have used potentials derived from an effective interaction almost identical to that used here. Renormalizations of about 0.90 ± 0.03 are found to be needed, in perfect agreement with the results obtained here for measurements at lower energies. Thus, a consistent description of the scattering over this whole energy range from 75 to 1120 MeV has been obtained, even though the apparent character of the scattering has evolved significantly.

In the two types of analyses we have performed, we encountered discrete ambiguities in the determination of the real potential. For the phenomenological analysis we studied three different families, which differed by the values of their volume integrals J_V, and have presented the results for one of them, family IV. The results for families III and V are qualitatively similar to the ones already discussed for family IV. The specially complicated structure of the angular distributions at the lower energies did not prevent these data from selecting discretely different strengths of the real part; this was more clearly seen in our microscopic analysis, probably because the real part depended only on one adjustable parameter. We interpret this sensitivity as an indication that the Airy pattern plays an important role in the symmetrized calculations at all the energies of this study.

Together with the deep real parts, rather weak absorption is required. This general feature is consistent with calculations [16] which predict for the symmetric α-structured systems $^{12}C+^{12}C$ and $^{16}O+^{16}O$ a remarkably low number of exit channels available to take away the incident flux. This should manifest itself in a very low absorption, as it is indeed the case. While the real part displays no important energy dependence, the absorption appears to change suddenly in the neighborhood of $E/A = 5.5$ MeV. At the higher energies of this study, the imaginary potential is mostly a soft-edge volume term, about 15 MeV at the center, volume integral about 65 MeV fm^3 and rms radius ≈ 5.2–5.5 fm. This is quite similar to what was found in the published analyses of the data at 124, 145, and 250 MeV [5,6,9]. However, at energies per nucleon below 5.5 MeV, the volume term becomes a thin-skinned ''box,'' plus an external Gaussian-like surface peak. Interestingly enough, the volume integral of this ''box + surface-peak'' imaginary potential is continuous with the mostly-volume description at the higher energies, even if their shapes are radically different, as Fig. 2 has shown. This is a welcome consistency of our description in terms of optical potentials, and adds a new element to the accumulated evidence of the importance of the volume integrals, real and imaginary, as significant indicators of the strength of the potential for light systems.

A change in the shape of the absorption in this energy region could be anticipated, as being the signature of reaction mechanisms evolving from fusion + direct reactions at the lowest energies (represented by the ''box + surface-peak'' imaginary potential) to a more spatially uniform absorption at energies near $E/A = 10$ MeV. (As a support for the interpretation, we can argue that measurements [31] of the contribution to the $^{16}O+^{16}O$ total reaction cross section from direct reactions, at $E_{\mathrm{c.m.}} = 26$ MeV, give a value $\approx 10\%$, which agrees quite nicely with the 15% of the total volume integral J_W contained into the surface derivative term at 75 MeV in this analysis.) We recall that this system needs a WSD imaginary term in addition to a soft-edged volume term again at about $E/A = 22$ MeV and above [7,8,30,32]. A complete calculation, including the effects of the coupling to the various reaction channels, might explain the features of these phenomenological results. In particular, the α structure of the nuclei involved suggests a possible strong effect from the coupling to the $^{20}Ne+^{12}C$ channel. Binary reactions were measured simultaneously to these elastic-scattering data, and once their analysis is completed [33], they might help explain the results encountered in this work. At the present time we do not have any suggestion why the change in the character of the imaginary potential near 90 MeV should occur so abruptly, particularly since fusion cross sections seem to have reached saturation at about 60 MeV [34,35].

The total reaction cross sections σ_R calculated with the relatively surface-transparent potentials shown in Fig. 2 are oscillating functions of the energy, similar to what has been observed in the already classic fusion measurements of some 20 years ago [34–38]. The theoretical oscillations are due, in this case of identical nuclei and surface-transparent potentials, to the successive participation of the even partial waves in the total absorption, and are not necessarily associated to a resonant process. Since the optical model σ_R are particularly sensitive to the exterior of the imaginary potential, where the scattering waves are largest, a detailed study might impose further constraints on potential parameters which are not completely determined by fitting the elastic-scattering data. However, such a study would require very accurate measurements of total reaction cross sections, which unfortunately are not available in this transitional region between the fusion-dominated low energies and the intermediate energy regime where direct measurements of σ_R could be possible.

Figure 6 shows the real and imaginary volume integrals for $^{16}O+^{16}O$ obtained from the analyses of this work, together with published values at higher energies. It can be observed that in this energy interval the overall strength of the real part, indicated by J_V, is very weakly dependent on energy, while the imaginary strength increases rapidly. In fact, J_W doubles its value over the energy interval of this study. At first sight these facts would seem to indicate a violation of the very general dispersion relation which connects the real and imaginary parts of the potential [10,11]. However, the curves in Fig. 6 show a three-linear-segment parametrization of the imaginary volume integral, and the

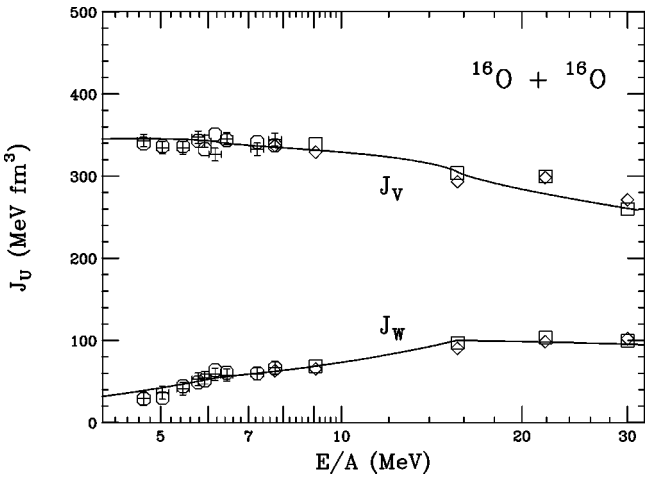

FIG. 6. Volume integrals for the potentials found in this study. Circles and crosses result from the phenomenological and microscopic analyses, respectively. Squares are the result of an independent folding model study [6] and diamonds show results from independent phenomenological [32,9,39] analyses at higher energies. The curve for J_W is a parametrization of the data and the curve for J_V is the dispersion relation prediction [10,11].

corresponding dispersion relation prediction for the variation of J_V with energy. The observed independence of J_V on the energy is consistent with the calculation, which predicts a broad, flat maximum value for J_V at E/A in the neighborhood of 6 MeV.

Qualitatively similar results have been reached in studies of $^{12}C+^{12}C$ [25] and $^{16}O+^{12}C$ [40] at approximately the same energies. Probably the most important differences between these systems are the details of the absorption. For $^{12}C+^{12}C$ a one-term (volume, Woods Saxon shape) imaginary part seemed to be sufficient to describe elastic scattering data between $E/A=6$ and 10 MeV. A two-component ''box+ surface-peak'' imaginary part, like that found in this analysis, was needed for $^{12}C+^{16}O$ at E/A between 4 and 8 MeV, with the surface term contributing as much as 60% of the total J_W at the highest energy. Again, calculations able to incorporate detailed nuclear structure and pertinent reaction mechanism information would be required to interpret these particular features of each system. In spite of the differences in their shape, the values of the real and imaginary volume integrals of the optical potentials for these three systems are similar, as well as their dependence on the energy.

We have used the near-far decomposition technique to interpret the angular distributions in terms of interfering trajectories. However, due to the low energies and the characteristics (strong attraction and very weak absorption) of the optical potentials encountered in this study, we have reached conditions where the technique begins to fail in the task of disentangling the complicated structure of the angular distributions. Since the scattering has evolved into conditions such that the refracted trajectories can be turned through more than 180°, a decomposition into only two types of contributions (from one or the other side), is no longer sufficient.

The analysis of the data presented here, which to our knowledge constitute the only complete elastic-scattering angular distributions measured in this energy range, has permitted to extend the mean-field description of the $^{16}O+^{16}O$ interaction down to energies of about 4 MeV/nucleon. Refractive effects are still important and permit a simple optical explanation for the main structures in the angular distributions and the deep minima observed in the excitation function. The real part of the interaction is well described by present folding model calculations, while the reported sudden change in the absorption requires, and deserves, further investigation.

S.S. and Z.B. want to express their gratitude to the Institut de Recherches Subatomiques, Strasbourg, for the warm hospitality during their stay. The work at Universidad Nacional Autónoma de México was partially supported by CONACYT 3039PE. Theoretical nuclear physics research at the University of Tennessee was supported by the U.S. Department of Energy through Contract Nos. DE-FG05-93ER40770 and DE-FG05-87ER40461. Oak Ridge National Laboratory is managed by Lockheed Martin Energy Research Corporation for the U.S. Department of Energy under Contract No. DE-AC05-96OR22464. S.S. acknowledges financial support through the French Embassy in Zagreb.

[1] M. E. Brandan, M. S. Hussein, K. W. McVoy, and G. R. Satchler, Comments Nucl. Part. Phys. **22**, 77 (1996).
[2] M. E. Brandan and G. R. Satchler, Phys. Rep. **285**, 143 (1997), and references therein.
[3] D. A. Goldberg and S. M. Smith, Phys. Rev. Lett. **33**, 715 (1974).
[4] E. Stiliaris, H. G. Bohlen, P. Fröbrich, B. Gebauer, D. Kolbert, W. von Oertzen, M. Wilpert, and Th. Wilpert, Phys. Lett. B **223**, 291 (1989); H. G. Bohlen, E. Stiliaris, B. Gebauer, W. von Oertzen, Th. Wilpert, M. Wilpert, A. N. Ostrowski, Dao T. Khoa, S. Demyanova, and A. A. Oglobin, Z. Phys. A **346**, 189 (1993).
[5] Y. Sugiyama, Y. Tomita, H. Ikezoe, Y. Yamamuchi, K. Ideno, S. Hamada, T. Sugimitsu, M. Hijiya, and Y. Kondō, Phys. Lett. B **312**, 35 (1993).
[6] Dao T. Khoa, W. von Oertzen, and H. G. Bohlen, Phys. Rev. C **49**, 1652 (1994).
[7] Dao T. Khoa *et al.*, Phys. Rev. Lett. **74**, 34 (1995).
[8] G. Barnitzky *et al.*, Phys. Lett. B **365**, 23 (1996).
[9] Y. Kondō, Y. Sugiyama, Y. Tomita, Y. Yamanouchi, H. Ikezoe, K. Ideno, S. Hamada, T. Sugimitsu, M. Hijiya, and H. Fujita, Phys. Lett. B **365**, 17 (1996).
[10] C. Mahaux, H. Ngo, and G. R. Satchler, Nucl. Phys. **A449**, 354 (1986).
[11] G. R. Satchler, Phys. Rep. **199**, 147 (1991).
[12] M. L. Halbert, C. B. Fulmer, S. Raman, M. J. Saltmarsh, A. H. Snell, and P. H. Stelson, Phys. Lett. **51B**, 341 (1974).
[13] K. W. McVoy and M. E. Brandan, Nucl. Phys. **A542**, 295

(1992).
[14] A. Morsad, F. Haas, C. Beck, and R. M. Freeman, Z. Phys. A **338**, 61 (1991).
[15] S. Szilner, Z. Basrak, R. M. Freeman, F. Haas, A. Morsad, M. P. Nicoli, and C. Beck, J. Phys. G **25**, 1927 (1999).
[16] F. Haas and Y. Abe, Phys. Rev. Lett. **46**, 1667 (1981); C. Beck, Y. Abe, N. Aissoui, B. Djerroud, and F. Haas, Phys. Rev. C **49**, 2618 (1994).
[17] See, for instance, K. A. Erb and D. A. Bromley, in *Treatise on Heavy-Ion Science*, edited by D. A. Bromley (Plenum, New York, 1985), and references therein.
[18] M. P. Nicoli *et al.*, Nucl. Phys. **A654**, 882c (1999).
[19] A. Meens, M. P. Nicoli, and D. Raiser, Nucl. Instrum. Methods Phys. Res. A **397**, 64 (1997).
[20] M. P. Nicoli, Ph.D. thesis, Université Louis Pasteur, Strasbourg, France, 1998; Institut de Recherches Subatomiques, Report IReS 98-16.
[21] M. H. Macfarlane and S. C. Pieper, Argonne National Laboratory Report No. ANL-76-11 (1978).
[22] Dao T. Khoa and W. von Oertzen, Phys. Lett. B **304**, 8 (1993).
[23] H. de Vries, C. W. de Jager, and C. de Vries, At. Data Nucl. Data Tables **36**, 495 (1987).
[24] Y. Kondō, F. Michel, and G. Reidemeister, Phys. Lett. B **242**, 340 (1990).
[25] M. E. Brandan, M. Rodríguez-Villafuerte, and A. Ayala, Phys. Rev. C **41**, 1520 (1990).
[26] R. C. Fuller, Phys. Rev. C **12**, 1561 (1975).
[27] K. W. McVoy and G. R. Satchler, Nucl. Phys. **A417**, 157 (1984).
[28] M. S. Hussein and K. W. McVoy, Prog. Part. Nucl. Phys. **12**, 103 (1984).
[29] N. Rowley, H. Doubre, and C. Marty, Phys. Lett. **69B**, 147 (1977).
[30] Dao T. Khoa, W. von Oertzen, and H. G. Bohlen (unpublished).
[31] H. H. Rossner, G. Hinderer, A. Weidinger, and K. A. Eberhard, Nucl. Phys. **A218**, 606 (1974).
[32] M. E. Brandan, K. W. McVoy, and G. R. Satchler, Phys. Lett. B **281**, 185 (1992).
[33] S. Szilner *et al.* (unpublished).
[34] B. Fernandez, C. Gaarde, J. S. Larsen, S. Pontoppidan, and F. Videbaek, Nucl. Phys. **A306**, 259 (1978).
[35] F. Saint-Laurent, M. Conjeaud, S. Harar, J. M. Loiseaux, J. Menet, and J. B. Viano, Nucl. Phys. **A327**, 517 (1979).
[36] J. J. Kolata, R. C. Fuller, R. M. Freeman, F. Haas, B. Heusch, and A. Gallmann, Phys. Rev. C **16**, 891 (1977).
[37] I. Tserruya, Y. Eisen, D. Pelte, A. Gavron, H. Oeschler, D. Berndt, and H. L. Harney, Phys. Rev. C **18**, 1688 (1978).
[38] D. G. Kovar *et al.*, Phys. Rev. C **20**, 1305 (1979).
[39] M. M. González and M. E. Brandan, contribution to *International Nuclear Physics Conference*, Paris, 1998, p. 287.
[40] M. P. Nicoli, F. Haas, R. M. Freeman, A. Morsad, S. Szilner, Z. Basrak, G. R. Satchler, and M. E. Brandan, Phys. Rev. C (to be published).